Optically transparent magnetic nanocomposites based on encapsulated Fe_3O_4 nanoparticles in a sol–gel silica network

Optically transparent magnetic nanocomposites based on encapsulated Fe_3O_4 nanoparticles in a sol–gel silica network

Senoy Thomas[1]**, D Sakthikumar**[2]**, P A Joy**[3]**, Yasuhiko Yoshida**[2] **and M R Anantharaman**[1,4]

[1] Department of Physics, Cochin University of Science and Technology, Cochin 682022, India
[2] Bio-Nano Electronics Research Centre, Department of Applied Chemistry, Toyo University, Kawagoe, Saitama 350-8585, Japan
[3] Physical Chemistry Division, National Chemical Laboratory, Pune, India

E-mail: senoythomas@yahoo.co.in and mra@cusat.ac.in

Abstract
Composite Fe_3O_4–SiO_2 materials were prepared by the sol–gel method with tetraethoxysilane and aqueous-based Fe_3O_4 ferrofluids as precursors. The monoliths obtained were crack free and showed both optical and magnetic properties. The structural properties were determined by infrared spectroscopy, x-ray diffractometry and transmission electron microscopy. Fe_3O_4 particles of 20 nm size lie within the pores of the matrix without any strong Si–O–Fe bonding. The well established silica network provides effective confinement to these nanoparticles. The composites were transparent in the 600–800 nm regime and the field dependent magnetization curves suggest that the composite exhibits superparamagnetic characteristics.

1. Introduction

Optically transparent magnetic materials have been the subject of many investigations during the past years because of their novel properties and potential applications. Among the most attractive properties of the transparent magnetic compounds are those related to the magneto-optical effects and their scientific and industrial applications in areas such as optical fibre sensors, optical isolators, information storage, magneto-optical switches, modulators, magnetic field and electric field sensors etc [1–3]. In addition to optical needs, the material must be integrated into the existing structures such as waveguides and optic fibres. As such, films and fibres are of great interest as the final form of these novel materials.

Nanocomposite materials show great promise as they can provide the necessary stability and processability for these important applications. In order to materialize the transparent magnetic composite within the limits of the visible range, it

is necessary to select an appropriate material as a matrix, which is optically isotropic and has an absorption edge in the UV region. Several groups have prepared transparent magnetic composites by using ion exchange resin, sol–gel synthesized aerogel and xerogel etc [4–7]. Ziolo *et al* reported the production of optically transparent magnetic composite for the first time. γ-Fe_2O_3 was grown in a polymeric ion exchange resin by introducing the Fe^{3+} and then exposing it to H_2O_2 at 60 °C [8]. The particles created ranged from 50 to 250 Å in size, which resulted in superparamagnetic properties. If the ion exchange resin was loaded multiple times, the particle size did not increase but the concentration of the particles did. The composite showed appreciable magnetization at and below room temperature. The highest saturation moment observed was 46 emu g^{-1} for 250 Å particles. Yamaguchi *et al* discussed work embedding magnetite in a PVA matrix [9]. These organic–inorganic composites are not capable of practical utilization, when chemical, thermal and mechanical durability is taken into consideration. Transparent glass containing magnetic

---

[4] Author to whom any correspondence should be addressed.

nanocrystals shows promising applications for magneto-optic devices. But most magnetic materials show an absorption edge in the visible range. Only small nanocrystals embedded in a transparent matrix could permit light transmission and avoid absorption and light scattering. A narrow size distribution of the magnetic particles and its homogeneous distribution over the matrix assure the achievement of composites with magnetic and optical homogeneity. It is important to reduce the size of the magnetic particles in the composite in order to obtain superparamagnetic behaviour allowing the sample to be used as low magnetic field sensors [10]. Besides particle size, the concentration of magnetic particles in the matrix and the thickness of the sample will both determine the magnetic and optical properties of the resulting composites. Thus, low amounts of magnetic particles in the matrix enhance the light transmission of the sample while diminishing its magnetic properties. Therefore, a compromise has been taken with regard to the concentration of the magnetic component in the matrix. The sol–gel process has some advantages for making this type of composite material for the following reasons. The process starts from liquid raw materials, so the precursors of magnetic fine particles such as ferric or ferrous salts can be easily and homogeneously mixed with a precursor of silica at the start of the experiment. This procedure enables us to precipitate magnetic fine particles within the pores of the silica matrix by a consequent thermal treatment. Several works are reported on the basis of this method of preparation [11–14]. The main problem arising with this type of preparation is the cracking of gels, so the end product will be in powdered form, and therefore it is impossible to measure their optical properties. Another peculiarity of the sol–gel process is that the dispersion medium gradually changes from liquid sol into solid gel. This shows that presynthesized magnetic fine particles can be dispersed into the silica sol and can be converted into the composite. The advantage of this process is that thermal treatment is not necessary and the problem of cracking of gels can be avoided. Yasumori *et al* prepared silica gel containing magnetite fine particles and measured their magneto-optical properties [15]. In this system, a homogeneous dispersion of the particles was not obtained as the magnetic particle settled down and were in the form of a film at the bottom of the silica gel. However, the method can be modified by using an aqueous-based ferrofluid of Fe_3O_4 as the magnetite precursor so that high homogeneity can be achieved. The present work reports on the preparation and characterization of a transparent magnetic nanocomposite utilizing an aqueous-based ferrofluid of Fe_3O_4 and its dispersion in silica sol. The composites were characterized by x-ray diffraction, FT-IR spectroscopy, transmission electron microscopy, UV–visible spectrometry and vibrating sample magnetometry. The results are presented here.

2. Experimental details

2.1. Preparation of Fe_3O_4 ferrofluid

A ferrofluid is a suspension of very fine magnetic particles with typical sizes of the order of 100 Å. For particles of this size, Brownian motion is sufficient to prevent sedimentation in a gravitational field. To prevent particle agglomeration through van der Waals attractive forces and magneto static inter particle
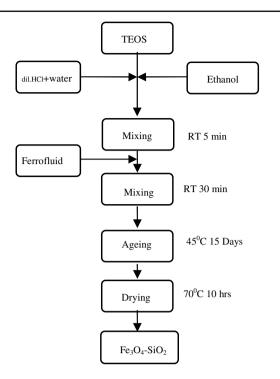
Figure 1. Schematic diagram of the experimental method.

interactions, the particles are generally coated with long chain polar molecules.

Aqueous ferrofluid was prepared by Massart's method [16]. For this, an aqueous mixture of ferric chloride (40 ml, 1 M) and ferrous chloride (10 ml, 2 M in HCl 2 M) was added to an ammonia solution (500 ml, 0.7 M). The gelatinous precipitate was isolated from the solution by magnetic decantation without washing with water. An alkali-based ferrofluid was made by peptizing the precipitate with aqueous 1 M tetra methyl ammonium hydroxide (TMAH).

2.2. Preparation of SiO_2 and Fe_3O_4–SiO_2 composite

The silica sol was prepared by mixing tetraethylorthosilicate TEOS, ethanol and water in the molar ratio 1:2:5. A few drops of dilute HCl were added as a catalyst to promote hydrolysis. The pH of the mixture was maintained at 2. The mixture was continuously stirred using a mechanical stirrer until a completely miscible solution was obtained. The viscous sol obtained was poured into a Petri dish and tightly covered. Holes were pierced in the cover of the dishes. The dishes were then kept in a hot air oven at 45 °C. The ageing period was 15 days. The monoliths thus obtained were densified by the heat treatment at 70 °C for 10 h. The sample is hereafter noted as S0.

The procedure for the preparation of monolithic silica was modified for obtaining composites by adding Fe_3O_4 ferrofluid to the silica sol. Fe_3O_4 nanocrystals were added into the silica sol considering both optical transparency and magnetic property. The experiment was repeated for 0.05 and 0.1 wt% Fe_3O_4 in silica. The samples are hereafter noted as SF: 0.05 and SF: 0.1 respectively. A schematic diagram of the experimental procedure is shown in figure 1.
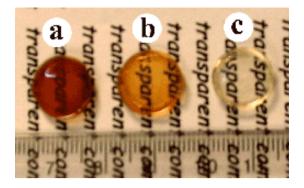
Figure 2. Photograph of the prepared composites (a) SF: 0.1, (b) SF: 0.05, (c) S0.

Figure 3. XRD pattern of precursor ferrofluid.

2.3. Characterization

The structural properties of the ferrofluid and Fe_3O_4–SiO_2 composites were analysed by an x-ray powder diffraction technique using a copper target (Cu Kα = 1.5418 Å, Rigaku D_{max} C). The scanning speed was adjusted to $2°$ min^{-1} with a sampling interval of 0.05. Transmission electron microscopy observations were carried out in a Joel JEM-2200 FS electron microscope operated at 200 kV. A Thermo Nicolete Avatar 370 DTGS model spectrophotometer using the KBr method was used in recording the FTIR spectra of the samples in the range 400–4000 cm^{-1}. The magnetization curves were recorded on a vibrating sample magnetometer (EG&G PAR model 4500 VSM) with an external field varying from -15 to 15 kOe. A Jasco V 530 UV–visible spectrometer was used to determine the optical transmittance of the composites in the wavelength range 300–800 nm with 1 nm resolution. All of these measurements were performed at room temperature.

3. Results and discussions

3.1. Structural analysis of Fe₃O₄–SiO₂ composites

The obtained monoliths were crack free. The samples were disc-shaped, approximately 1 cm in diameter and 1 mm thick. The transparency of the samples decreased with increasing Fe_3O_4 percentage. Figure 2 shows the photograph of the prepared samples. There is no visible segregation of particles in the monoliths prepared.

The crystallinities of ferrofluids and Fe_3O_4–SiO_2 composites were examined by XRD studies. Figures 3 and 4 show the XRD patterns of ferrofluids and Fe_3O_4–SiO_2 composite respectively. The XRD pattern of the ferrofluid has all lines corresponding to Fe_3O_4 (JCPDS 19-0629) and it exists in an inverse spinel form which is the characteristic of magnetite. There are six main peaks observed clearly in the XRD pattern of ferrofluid. The diffraction peaks are at $2\theta \sim 30.25$ (220), $2\theta \sim 35.75$ (311), $2\theta \sim 43.55$ (400), $2\theta \sim 53.7$ (422), $2\theta \sim 57.45$ (511), $2\theta \sim 62.70$ (440).

The average lattice parameter calculated at different 2θ values corresponding to different peaks in the XRD spectrum was 8.334 Å. The diameter (D) of the nanoparticles was estimated from the FWHM of the main peak of Fe_3O_4 (311)
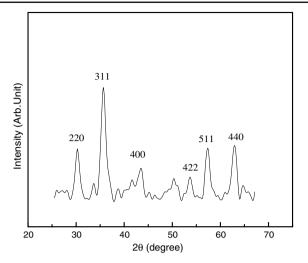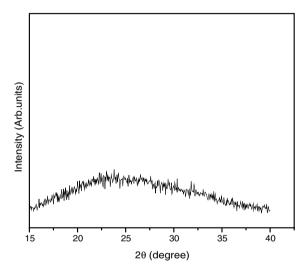

Figure 4. XRD pattern of the representative Fe₃O₄–SiO₂ composite.

by using the relation

$$D = \frac{0.9\lambda}{\beta_{1/2}\cos\theta}$$

where λ is the wavelength of Cu Kα radiation and $\beta_{1/2}$ is the FWHM of the x-ray peak (311). This analysis gives the diameter of the nanoparticles as about 14 nm.

The XRD pattern of Fe_3O_4–SiO_2 composites exhibited a broad diffraction band centred on a two theta value of $25°$, which corresponds to amorphous SiO_2. The silica is clearly noncrystalline but the short range correlation results in a very broad peak centred at a two theta value of $25°$. Lines of Fe_3O_4 are not prominent in the diffraction pattern due to the dilution of Fe_3O_4 in SiO_2.

Figure 5 shows a TEM image of the Fe_3O_4–SiO_2 composite. The dark contrast aggregates visible in the TEM images are crystalline Fe_3O_4 clusters. The mean particle diameter evaluated from the figure was found to be 20 nm. There is a small discrepancy in the value of grain size obtained from TEM and x-ray analysis, which may be due to the size
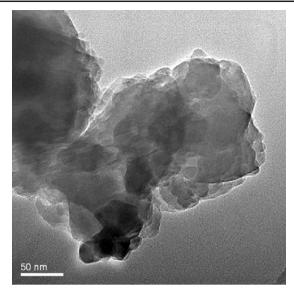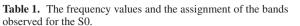
Figure 5. TEM image of the Fe_3O_4–SiO_2 composite.

Table 1. The frequency values and the assignment of the bands observed for the S0.

Frequency (cm^{-1})	Assignment
460	δ (O–Si–O)
798.23	ν_s (Si–O–Si)
955.13	ν Si–OH
1081.47	ν_{as} (Si–O–Si)
1644.4	δ H_2O
3507.88	ν (OH) of bonded silanol groups

Table 2. The frequency values and the assignment of the bands observed for the representative Fe_3O_4–SiO_2 composite.

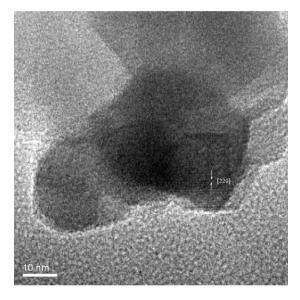| Frequency (cm^{-1})	Assignment
455	δ (O–Si–O)
564	(Fe–O)
664	(Fe–O)
797	ν_s (Si–O–Si)
961	ν Si–OH
1078	ν_{as} (Si–O–Si)
1658	δ H_2O
3472	ν H_2O

Figure 6. HRTEM image of the representative composite.

distribution present in the system. Detailed HRTEM and mapping of elements (figures 6 and 7) were conducted for the composite to determine the nature of the crystallite aggregates that were observed. Lattice planes of the aggregates are easily recognizable and the high resolution of the image permitted them to be assigned to the Fe_3O_4(220) plane. From the mapping and HRTEM studies, we can conclude that the Fe_3O_4 is placed as nanocrystals in the composites and it is surrounded by amorphous silica.

The nature of bonding present in SiO_2 and Fe_3O_4–SiO_2 can be observed by the FTIR spectra presented in figures 8 and 9. Figure 8 shows the FTIR spectrum of the pure silica gels. The IR spectrum of the silica gel is characterized by three main absorption bands assigned to different vibrational modes of the Si–O–Si bonds. The lowest frequency mode ($\sim$460 cm^{-1}) is assigned to transverse-optical (TO) rocking motions perpendicular to the Si–O–Si plane, of the oxygen bridging two adjacent Si atoms. A weak band is observed near $\sim$800 cm^{-1} due to symmetric stretching of the O atom along a line bisecting the Si–O–Si angle. The highest frequency mode $\sim$1200 cm^{-1}, 1075 cm^{-1} involves motion back and forth of the oxygen atom along a line parallel to the Si–Si axis [17, 18]. The motion results in opposite distortion of two neighbouring Si–O bonds. The frequency values and the assignment of the bands observed for the SiO_2 sample are listed in table 1.

The band at 1644 cm^{-1} is due to the bending of the absorbed H_2O molecules, which can interact through hydrogen bonds with silanol groups [17]. The characteristic band for stretching (OH) groups was found around 3500 cm^{-1} [19].

An FTIR spectrum of a Fe_3O_4–SiO_2 composite is shown in figure 9. The spectrum has all characteristic bands of silicon dioxide as seen in the pure case. The difference is the peaks seen at 564 and 664 cm^{-1}. This is due to Fe–O vibrations in octahedral and tetrahedral sites of Fe_3O_4 respectively [20, 21]. Not all bands of Fe_3O_4 are obtained due to instrument limits. It is also interesting to note the absence of a band at 857 cm^{-1} in the spectrum, which suggests that no Si–O–Fe bonds are formed [19]. From this result, it can be concluded that no strong bond exists between Fe_3O_4 and silica and therefore Fe_3O_4 exists within the pores of the silica gel without any strong Si–O–Fe bonding. The frequency values and the assignment of the bands observed for the composite samples are shown in table 2.

Thus, the well established silica network provides effective confinement to Fe_3O_4 nanoparticles. The absence of strong Si–O–Fe bonding can be attributed to two factors. The synthesis of the magnetic composites at a relatively low temperature ($\sim$70 °C) does not help in the formation of the Si–O–Fe bonds. Secondly, we are adding presynthesized Fe_3O_4 nanoparticles to the silica sol and the silica network is only entrapping or immobilizing these nanoparticles.

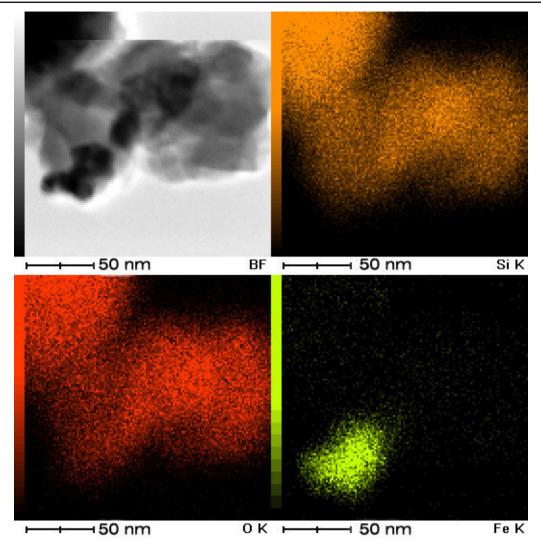The process of embedding magnetic nanoparticles can be schematically represented by figure 10. Here, the entire

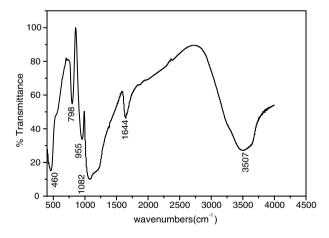**Figure 7.** Mapping of the elements in the Fe$_3$O$_4$–SiO$_2$ composite.

Figure 8. FTIR spectrum of the pristine sample S0.

Figure 9. FTIR spectrum of the representative Fe$_3$O$_4$–SiO$_2$ composite.

sol–gel process can be represented by the following chemical reactions.

$$\equiv\text{Si–OR} + \text{H}_2\text{O} \Leftrightarrow \equiv\text{Si–OH} + \text{ROH}$$

$$\equiv\text{Si–OR} + \text{HO–Si}\equiv \Leftrightarrow \equiv\text{Si–O–Si}\equiv + \text{ROH}$$

$$\equiv\text{Si–OR} + \text{HO–Si}\equiv \Leftrightarrow \equiv\text{Si–O–Si}\equiv + \text{H}_2\text{O}$$
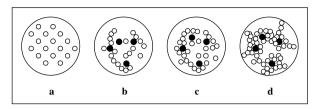
Figure 10. The entrapment of magnetic nanoparticles in the silica matrix. (a) Formation of the sol particles during the hydrolysis and condensation stages. (b) Addition of the magnetic nanoparticles into the sol. (c) Trapping of the magnetic nanoparticles by the growing silica network. (d) Immobilization of the magnetic nanoparticles in the silica matrix.

where R is the alkyl group. Hydrolysis of alkoxysilanes leads to the formation of silane. Their condensation with each other or with alkoxysilanes results in the formation of siloxanes. Linkage of additional =Si–OH tetrahedra occurs as the polycondensation reaction proceeds. The initiation of hydrolysis and the polycondensation reaction occurs at numerous sites within the TEOS + H_2O solution as mixing proceeds. When sufficient interconnected Si–O–Si bonds are formed in a region they respond comparatively as colloidal particles or as sol as shown in figure 10(a). Sol is a low viscosity liquid. The magnetic nanoparticles are added at this stage (figure 10(b)). With time, the colloidal particles and condensed silica matter link together to become a 3D network. The magnetic particles situated between these sol particles get trapped within the growing silica network (figure 10(c)). The physical characteristics of the gel network depend greatly upon the size of particles and the extent of cross-linking prior to gelation. At gelation, the viscosity increases sharply and a solid object results in the shape of the mould. Further linkage occurs during the final stages of ageing and the magnetic nanoparticles get immobilized in the resulting silica network (figure 10(d)).

3.2. Magnetic properties

In a ferrofluid, each particle is a magnetic single domain of magnetic moment μ given by [22]

$$\mu = \frac{4M_s \mu_0 \pi a^3}{3} \qquad (1)$$

where M_s is the saturation magnetization of the bulk material, 'a' is the radius of the particle and μ_0 is the permeability of free space.

In the absence of any magnetic field, the magnetic moments μ have a random orientation, and the net average magnetization of the fluid is zero. When a magnetic field is applied, there is a tendency for the particles to align in the direction of the magnetic field. Langevin's theory of paramagnetic gases applies to the ferrofluids provided that the magnetic field interactions are negligible. This behaviour of the magnetic fluids is known as superparamagnetism. The statistical average of the magnetic moments μ is oriented along the magnetic field and its amplitude is
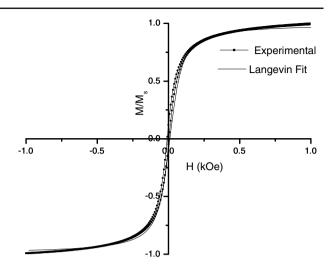
$$\overline{\mu} = \mu L(x) \qquad (2)$$

Figure 11. Normalized magnetization curve for ferrofluid.

where $x = \frac{\mu H}{k_B T}$ for an applied magnetic field H and $L(x)$ is the Langevin function. It is recalled that $L(x) = \coth x - \frac{1}{x}$ and $L(x) = \frac{x}{3}$ for $x \ll 1$. This expression assumes that the system consists of noninteracting and monodispersed particles. Quantitative comparisons with experiments have shown that a polydispersity function should be added to (2).

The normalized magnetization curve for ferrofluids well fits with the Langevin function as shown in figure 11. The curve was drawn assuming that the system consists of noninteracting and monodispersed particles. For fitting the Langevin function, a particle diameter of 10 nm was assumed. A small deviation from the fit indicates that a size distribution is present within the ferrofluids. The saturation magnetization M_s for ferrofluid is 56 emu g^{-1}. An M_s value less than that of the bulk Fe_3O_4 reflects the small particle size of Fe_3O_4 nanocrystals. Spin canting as well as the order disorder characteristic of the particles has been reported to be responsible for the reduction in M_s manifested by nanoparticles [23]. The hysteresis loops at room temperature for the two Fe_3O_4–SiO_2 nanocomposites with 0.05 and 0.1 wt% magnetite show field dependent magnetization curves typical of ultra fine magnetic composites. The hysteresis loops for the two samples at room temperature are presented in figure 12. The saturation magnetization value, M_s increases from 0.03 to 0.06 emu g^{-1} as the concentration of the magnetite in the matrix increases from 0.05% to 0.1%. The value of coercivity noted for SF: 0.05 and SF: 0.1 are 37 and 72 Oe respectively.

3.3. Optical properties

Figure 13 shows the transmittance spectrum for silica as well as the composites. The composites are optically transparent in the 600–800 nm regime. The relative transmittance of the sample SF: 0.05 is 56% and that of SF: 0.1 is 19% when compared to S0. It should be noted here that the samples were not polished prior to optical measurements. Hence, here surface roughness can aid light scattering, which plays a key role in the transmittance of the samples. Besides surface roughness, air filled pores can also contribute to scattering. The presence
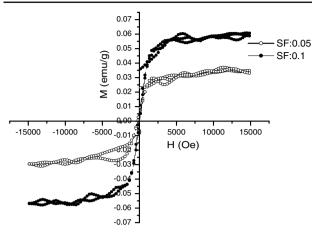
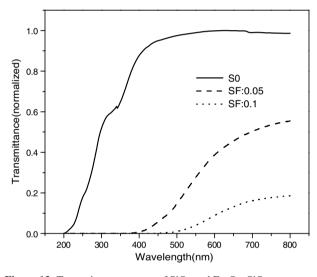**Figure 12.** Room temperature magnetization curves for composites.

Figure 13. Transmittance spectra of SiO$_2$ and Fe$_3$O$_4$–SiO$_2$ composites.

Figure 14. TEM image of a Fe$_3$O$_4$–SiO$_2$ composite. Arrow shows empty pores.

4. Conclusions

In conclusion, we have demonstrated that it is possible to obtain transparent magnetic nanocomposites by the entrapment of magnetic nanoparticles within the sol–gel silica network. Spectral studies showed the presence of Fe$_3$O$_4$ within the pores of the silica matrix and suggest that a well established silica network provides effective confinement to Fe$_3$O$_4$ nanoparticles. The magnetic nanoparticles are within the pores of the silica matrix without any strong Si–O–Fe bonding. The composites are superparamagnetic in nature and the magnetization of the composites depends on the concentration of the magnetic nanoparticles in the matrix. The obtained monoliths were crack free and were transparent in the 600–800 nm regime. Moreover, the preparation method promises to obtain monoliths of any shape. Due to this combination of properties, this material can be considered as a potential candidate for magneto-optical applications. Furthermore, during the synthesis, particles can be aligned under an applied external magnetic field resulting in an oriented direction in a non-magnetic matrix. Thus, anisotropy can be created and further scope exists in making permanent birefringent components using this technique.

of unfilled pores is evident from the transmission electron micrograph (figure 14). It may be noted here that Zayat *et al* used PHEMA as a refractive index matching material in the empty pores and they obtained a better transparency for a composite of smaller thickness (0.33 mm). However, it is to be noted here that the transparent composite samples used in this investigation were crack free monoliths of 1 mm thick. A comparison of the absorption edge between SiO$_2$ and Fe$_3$O$_4$–SiO$_2$ shows an obvious red shift in Fe$_3$O$_4$–SiO$_2$ composites. The large red shift of optical absorption edge is considered to be due to two factors. One of these comes from the mixing effect of the bandgap of the composites. When SiO$_2$ with a relatively higher bandgap is mixed with a low bandgap Fe$_3$O$_4$, the bandgap of Fe$_3$O$_4$–SiO$_2$ composites will be located between the band gap of these two materials, that is it shifts to lower energy compared to SiO$_2$. The other factor to be considered is the surface and interface effect between Fe$_3$O$_4$ and SiO$_2$ particles [24, 25]. A higher concentration of Fe$_3$O$_4$ nanoparticles in silica strengthens such effects and therefore leads to the red shift of the absorption edge as shown in figure 13.
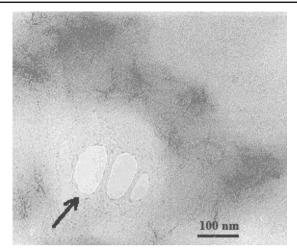
References

[1] Guerrero H, Rosa G, Morales M P, del Monte F, Moreno E M, Levy D, Perez del Real R, Belenguer T and Serna C J 1997 *Appl. Phys. Lett.* **71** 2698

[2] Beecroft L L and Ober C K 1997 *Chem. Mater.* **9** 1302

[3] Qiu J and Hirao K 1996 *Japan. J. Appl. Phys.* **35** L1677

[4] Malini K A, Anantharaman M R, Sindhu S, Chinnasamy C N, Ponpandian N, Narayanasamy A, Balachandran M and Sivasankara Pillai V N 2001 *J. Mater. Sci.* **36** 821

[5] Nair S S, Mathews M and Anantharaman M R 2005 *Chem. Phys. Lett.* **406** 398

[6] Gich M *et al* 2003 *Appl. Phys. Lett.* **82** 4307

[7] Bentivegna F, Nyvlt M, Ferre J, Jamet J P, Brun A, Visnovsky S and Urban R 1999 *J. Appl. Phys.* **85** 2270

[8] Ziolo R F, Giannelis E P, Weinstein B A, O'Horo M P, Ganguly B N, Mehrotra V, Russell M W and Huffman D R 1992 *Science* **257** 219

[9] Yamaguchi K, Matsumoto K and Fujii T 1990 *J. Appl. Phys.* **67** 4493

[10] Zayat M, del Monte F, del Puerto Morales M, Rosa G, Guerrero H, Serna C J and Levy D 2003 *Adv. Mater.* **15** 1809

[11] del Monte F, Morales M P, Levy D, Fernandez A, Ocana M, Roig A, Molins E, O'Grady K and Serna C J 1997 *Langmuir* **13** 3627

[12] Cannas C, Gatteschi D, Musinu A, Piccaluga G and Sangregorio C 1998 *J. Phys. Chem.* B **102** 7721

[13] Jitianu A, Crisan M, Meghea A, Rau I and Zahareseu M 2002 *J. Mater. Chem.* **12** 1401

[14] Battisha I K, Afify H H and Hamada I M 2005 *J. Magn. Magn. Mater.* **292** 440

[15] Yasumori A, Matsumoto H, Hayashi S and Okada K 2000 *J. Sol–Gel Sci. Technol.* **18** 249

[16] Massart R 1981 *IEEE Trans. Magn.* **17** 1247

[17] Bruni S, Cariati F, Casu M, Lai A, Musinu A, Piccaluga G and Solinas S 1999 *Nanostruct. Mater.* **11** 573

[18] Innocenzi P 2003 *J. Non-Cryst. Solids* **316** 309

[19] Moreno E M, Zayat M, Morales M P, Serna C J, Roig A and Levy D 2002 *Langmuir* **18** 4972

[20] Ardelean I, Andronache C, Cimpean C and Pascuta P 2004 *Mod. Phys. Lett.* B **18** 45

[21] Gillot B and Bouton F 1980 *J. Solid State Chem.* **32** 303

[22] Lacoste D, Donatini F, Neveu S, Serughetti J A and Van Tiggelen B A 2000 *Phys. Rev.* E **62** 3934

[23] Morales M P, Veintemillas-Verdaguer S, Montero M I and Serna C J 1999 *Chem. Mater.* **11** 3058

[24] Zhou Z H, Xue J M, Chan H S O and Wang J 2001 *J. Appl. Phys.* **90** 4169

[25] Li G-H, Wu Y-C and Zhang L-D 2001 *Chin. Phys.* **10** 148